

A MACHINE VISION SYSTEM FOR QUANTIFICATION OF CITRUS FRUIT DROPPED ON THE GROUND UNDER THE CANOPY

D. Choi, W. S. Lee, R. Ehsani, F. M. Roka

ABSTRACT. *The overall goal of this study was to develop a machine vision system to quantify dropped citrus fruits on the ground. Specific objectives were: (1) to build a machine vision system suitable for citrus grove field conditions, (2) to develop an image enhancement algorithm for varying illumination conditions, and (3) to develop an image processing algorithm to estimate citrus fruit drop count and mass. The image processing algorithm consisted of (1) illumination enhancement using a retinex algorithm, (2) classification, (3) segmentation using a watershed algorithm with h-minima transform, and (4) ellipse fitting for mass estimation. Performances of the algorithms were evaluated in terms of correct identification and false positive errors. The average correct identification rate was 88.1%, 83.6%, and 82.9% for logistic regression, k-nearest neighbor (kNN), and Bayesian classifiers, respectively. False positive errors were 13.7%, 40.9%, and 17.9% for logistic regression, kNN, Bayesian classifiers, respectively. The results demonstrate the system's ability to quantify dropped fruits with specific geo-referenced location information. Spatially varied fruit drop maps plotted from the results can assist growers in finding problematic areas in their citrus groves more efficiently while reducing inspection and treatment costs. Such maps can also facilitate treatment of citrus Huanglongbing (HLB) disease in combination with HLB intensity data, psyllid counts, fertilization programs, and other block-specific management practices.*

Keywords. *Computer vision, Geo-referenced mapping, Image enhancement, Image processing, Precision agriculture, Retinex, Watershed algorithm.*

Premature citrus fruit drop is a serious concern that negatively affects crop yield. Fruit drop can have various causes, including inadequate drainage, nutritional deficiencies, and extreme weather conditions with respect to rain and temperature (Begeman and Wright, 2009). Sometimes a combination of unfavorable environmental factors and diseases causes severe fruit drop. For instance, inadequate irrigation combined with warm temperatures can create an outbreak of brown rot disease, which can cause as much as 25% of the entire crop to drop off the trees (Zekri and Rouse, 2013). The citrus industry in the U.S., particularly in Florida, is under a significant threat from an exotic disease called Huanglongbing (HLB), which is also known as citrus greening. HLB has spread throughout Florida and started to infect citrus trees in Texas and California. This disease is considered a main reason for

unexpected and excessive premature citrus fruit drops that consequently decrease yields (Bassanezi et al., 2011). During the 2013-2014 season, more than 11% of citrus production in Florida was lost due to the early drop caused by both HLB and unfavorable weather (USDA, 2014).

Methods that accurately quantify and geo-reference the intensity of fruit drop could have significant economic value to citrus growers. First, fruit drop data would enable crop production estimates to be revised more accurately and timely during the course of a harvest season. Second, fruit drop data could assist growers in scheduling harvest to minimize fruit losses from the most affected blocks. Third, spatially referenced fruit drop data could be correlated with HLB infection rates and psyllid counts along with block-specific management practices, such as fertilization programs and irrigation schedules, to more effectively diagnose and minimize fruit drop from HLB-inflected areas. Presently, fruit drop data are collected by sampling random areas within a block and manually counting dropped fruit. This method is costly and time consuming. Growers in Florida are asking for new tools that will allow them to quickly and accurately quantify fruit drop with geo-referenced location information.

Machine vision is commonly used as an automatic non-destructive visual inspection tool (Aleixos et al., 2002), especially in the production of delicate fruit such as citrus, blueberries, apples, and tomatoes. Recently, many studies using machine vision techniques have been reported for sorting fruit and yield estimation, including fruit detection

Submitted for review in March 2014 as manuscript number ITSC 10688; approved for publication by the Information, Technology, Sensors, & Control Systems Community of ASABE in May 2015. Presented at the 2013 ASABE Annual Meeting as Paper No. 131591603.

The authors are **Daeun Choi, ASABE Member**, Graduate Research Assistant, and **Won Suk Lee, ASABE Member**, Professor, Department of Agricultural and Biological Engineering, University of Florida, Gainesville, Florida; **Reza Ehsani, ASABE Member**, Associate Professor, Citrus Research and Education Center, University of Florida, Lake Alfred, Florida; **Fritz M. Roka**, Associate Professor, Southwest Florida Research and Education Center, University of Florida, Immokalee, Florida. **Corresponding author:** Won Suk Lee, 207 Frazier Rogers Hall, P.O. Box 110570, Gainesville, FL 32611; phone: 352-392-1864, ext. 207; e-mail: wslee@ufl.edu.

and mass estimation (Yang et al., 2012), disease detection (Li et al., 2014; Pourreza et al., 2013), and robotic harvesting (Ling et al., 2004). For fruit detection and mass estimation using a closed imaging system, several machine vision applications have been studied. Chinchuluun et al. (2009) developed a machine vision system to identify citrus fruit and its size on a canopy shake and catch harvester during harvesting. The citrus detection and size identification algorithm included a Bayesian classifier using color information and watershed segmentation. The total area of citrus fruit was measured, yielding an R^2 value of 0.892 between citrus fruit count and actual mass. Shin et al. (2012) developed a system for postharvest citrus mass estimation. Color information was used for citrus detection. A highly saturated area recovering algorithm (HSAR) and watershed algorithm using h -minima transform were used to identify the number of fruit and fruit sizes.

Fruit recognition using outdoor images in open areas, however, is challenging because object colors in images vary greatly under different illumination conditions. Many studies of fruit detection in outdoor images have shown reduced performance (Annamalai and Lee, 2003; Annamalai et al., 2004; Stajanko et al., 2004; Patel et al., 2012). Annamalai and Lee (2003) developed a citrus yield mapping system using machine vision with outdoor imaging. The acquired images were converted to the hue, saturation, and value (HSV) color space, and then fruit objects were segmented using erosion, dilation, and thresholding. A connected component was considered a fruit. However, the segmentation using thresholding, erosion, and dilation caused underestimation because some groups of fruit were not segmented properly using thresholding and were considered one fruit. Their results showed a coefficient of determination (R^2) of 0.76 between counting by the algorithm and the actual number of fruit. Annamalai et al. (2004) developed a real-time system for outdoor imaging for estimation of citrus yields and reported an R^2 value of 0.79 between the number of fruit counted by the algorithm and the actual number of fruit. This research showed better results than the previous study even though they also used thresholding for the segmentation. After segmentation, they differentiated single fruit and groups of fruit according to the number of pixels that belonged to an object. However, it was not possible to count more than two fruits if a group had three or more fruits. They also noted problems with uneven illumination and fruit occlusion. Stajanko et al. (2004) developed a method to estimate the number and sizes of fruit in an apple orchard. Thermal images were used for the fruit detection algorithm, and morphological operations, such as erosion and dilation, were used for segmentation. They mentioned limitation of segmentation due to the simplicity of the morphological operation, so it was not possible to segment apples accurately. The R^2 value ranged from 0.83 to 0.88 between the actual number of fruit and estimation by the algorithm. Patel et al. (2012) suggested automatic segmentation for yield estimation of various fruit on trees, such as citrus, apple, pomegranate, peach, and plum, using color and shape. Color information of the a component in the L^*a^*b color space (lightness and

color channels a and b ; HunterLab, 2012) were used to detect fruit regions. Circle fitting was performed to find fruits in the images. However, the average error in the validation set was 31% because many of clusters were counted as a single fruit due to the lack of a segmentation process.

The overall goals of this study were to develop a machine vision system using outdoor RGB images to correctly count citrus fruit dropped on the ground and estimate their mass, which can be used in creating a geo-referenced fruit drop map. Specific objectives of the research were:

1. To build a machine vision system suitable for field conditions in citrus groves.
2. To develop an image enhancement algorithm to address problems from variable illumination.
3. To develop an image processing algorithm that can estimate dropped fruit count and mass.

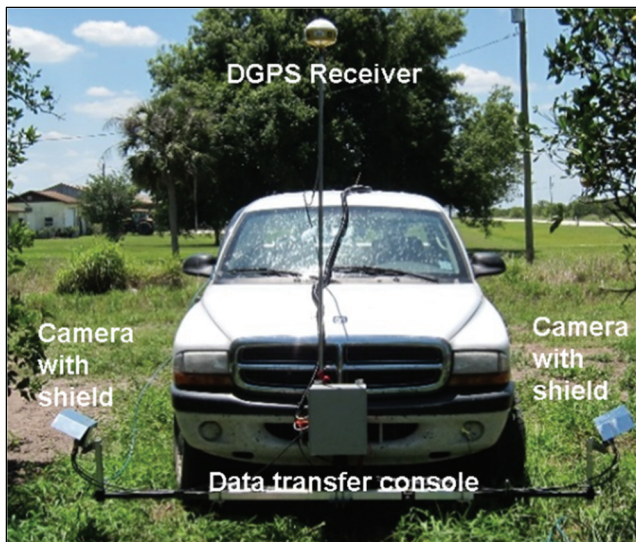
MATERIALS AND METHODS

IMAGE ACQUISITION HARDWARE

An outdoor imaging system was designed and constructed with two RGB cameras (NI-1772C, National Instruments Corp., Austin, Tex.) that were equipped with microprocessors (1.6 GHz Intel Atom). Each cameras had a 1/3 in. CCD sensor with 640×480 resolution and a lens with 3.5 mm focal length ($f1.4$, GM23514MCN, Goyo Optical, Inc., Asaka, Japan). The relatively low-resolution cameras were used to reduce the image processing time since the system was required to inspect large areas of a commercial citrus grove. The cameras were designed to work in the field conditions typically found in a citrus grove, i.e., dusty and humid with high temperatures. Metal shields were installed on top of the cameras to protect them from damage by tree branches and dew (fig. 1a). The cameras were mounted on both sides of the front of a pickup truck. The cameras had digital input/output channels including RS-232 serial communication and a digital pulse detector. These channels were used to transfer digital data from a rotary encoder (4096 pulses, Stegmann CI20, Bloomington, Minn.; fig. 1b) and a DGPS receiver (AgGPS 132, Trimble Navigation, Ltd., Sunnyvale, Cal.; fig. 1a) to the cameras. Encoder readings were used as external triggers to acquire images with the same distance between images regardless of the speed of the truck. The DGPS receiver was used to record time and position whenever an image was acquired. When the imaging system was triggered to acquire a new image, a GGA sentence defined by the NMEA 0183 standard was saved. Image acquisition software was developed using Labview (National Instruments Corp., Austin, Tex.) and installed in the processors in the cameras.

IMAGE ACQUISITION IN A CITRUS GROVE

Images were acquired on May 15 and 16, 2013, in a commercial citrus grove (Lykes Bros., Inc., Ft. Basinger, Fla.). As the truck moved forward at an average speed of 8 km h^{-1} , a total of 180 images were taken at three illumination levels: 60 images each at dark, medium, and bright illumination (as discussed further under "Illumination Enhancement Using Retinex Algorithm"). The exposure time



(a)



(b)

Figure 1. Hardware setup: (a) DGPS receiver and two cameras attached to mounting frame and (b) encoder mounted on a small trailer behind the truck.

was fixed at 5 ms without gain. Each image's field of view was 7 m × 4.6 m and contained dropped citrus fruit on the ground, especially under the canopy area. The lowest canopy was about 46 cm above the ground, so the cameras were installed at 50 cm height and tilted downward at an angle of 60° (fig. 2). Twenty images were selected as the training set for each illumination level, and the other 40 images were used as the validation set.

IMAGE PROCESSING ALGORITHM DEVELOPMENT

The image processing algorithm was developed using Matlab (The MathWorks, Inc., Natick, Mass.). The major processing steps of the algorithm included improving illumination using a retinex algorithm, classifying citrus fruit from the background using different types of classifiers, and estimating counts and mass of the detected fruit. A flowchart for the algorithm is shown in figure 3.



Figure 2. Downward angle of camera (with metal shield removed).

ILLUMINATION ENHANCEMENT USING RETINEX ALGORITHM

Shading within the grove created varying levels of illumination in the images. The illumination levels were calculated by averaging the gray values (an average of the R, G, and B components) of all the pixels in an image. Based on observation of the training images, the illumination levels in images ranged from 30 to 210. The images were divided into three groups based on illumination level: 30 to 90 (dark), 90 to 150 (medium), and 150 to 210 (bright). The different illumination levels of the images created the most critical problem for the performance of the algorithm due to the dramatic changes in the color values of objects. For example, in figure 4, citrus fruit at the three illumination levels, dark, medium, and bright (figs. 4a, 4b, and 4c), had significantly different RGB values. Citrus fruit under dark illumination, due to cloud cover, was almost brown with average RGB values of (48, 41, 29), and there was no distinctive color variation between the background and the fruit. However, at medium and bright illumination, the citrus fruit had orange color (average RGB of 108, 98, 72) and bright yellow color (average RGB of 229, 191, 138), respectively.

For reliable classification, a single-scale retinex algorithm was applied to reduce the color variation between images with different illumination. According to the retinex algorithm, independence of colors from the illumination can be achieved by correlating the reflectance of red, green, and blue signals regardless of the amount of illumination. The theory of the independence of colors from the illumination can be expressed by equation 1 (Rahman, 1995):

$$R_k(m,n) = \log I_k(m,n) - \log [F(m,n) * I_k(m,n)] \quad (1)$$

where (m,n) is the pixel index, $R_k(m,n)$ is the retinex output, $I_k(m,n)$ is the k th spectral band distribution of the image, $F(m,n)$ is a surrounded function that defines the neighborhood of a pixel, and $*$ is a convolution operation. In this study, a Gaussian function was used as the surrounded function and is defined by:

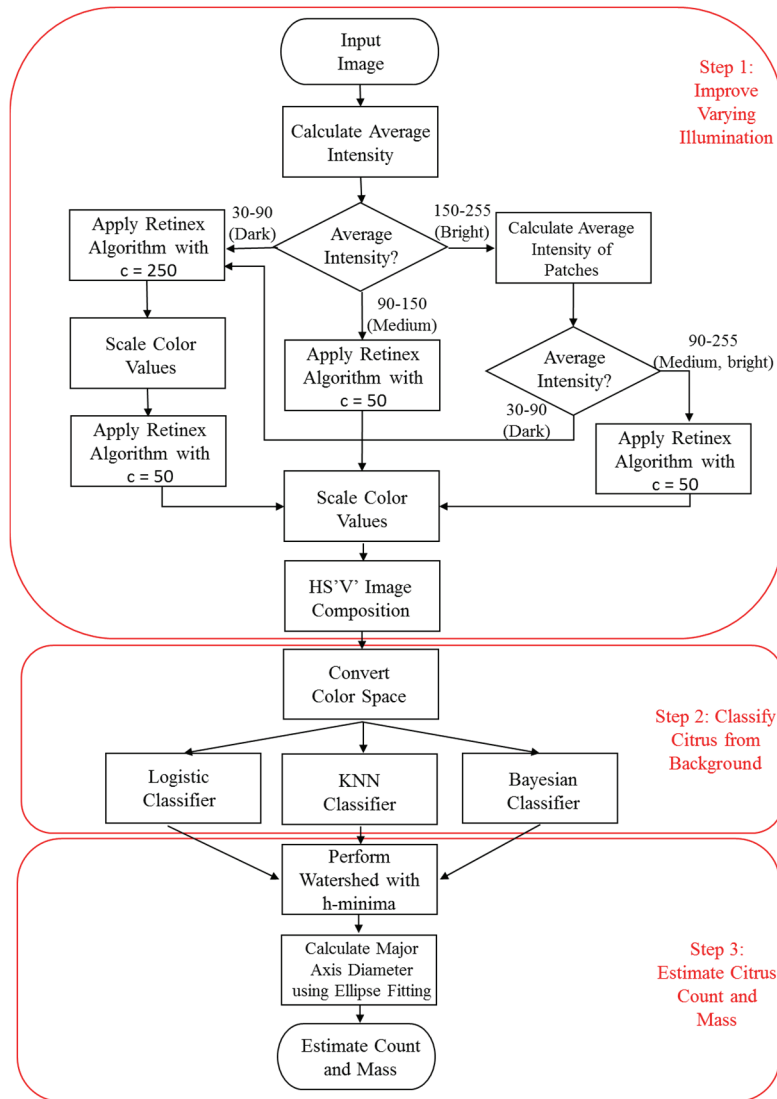


Figure 3. Flowchart of the proposed image processing algorithm showing three major steps: (1) illumination enhancement, (2) classification of citrus fruit from the background, and (3) count and mass estimation.

$$F(x, y) = Ke^{\left(\frac{x^2 + y^2}{c}\right)} \quad (2)$$

where $K = 1/\iint F(x, y) dx dy$, and c represents the standard deviation of the Gaussian function.

The standard deviation (c) was chosen depending on the illumination level. Dark images had consistently low illumination in the entire image, and so a larger c value (250) was chosen to tolerate the global effect of illumination and reduce the phenomenon by which color becomes lighter due to white shade. The white shade problem became more noticeable when a smaller c value was used. However, the problem was resolved by color scaling, which is adjusting color values not to exceed 255. Another retinex operation was then performed to achieve better illumination, i.e., enough to recognize objects but not varying for classification process.

Images with medium or bright illumination contained areas with and without shadow. For medium illumination, c was chosen to be small (50) to allow regional calculation of the illumination effect because the typical shadow area in

the images was about 50×50 pixels. In the bright illumination images, illumination gaps between areas with and without shadow were too big to be enhanced by applying a uniform c value to the entire image. For this reason, the bright illumination images were divided into 24 image sections of 20×640 pixels each. Depending on the average illumination of each section, a value of 50 was chosen for non-shadow areas and 250 was chosen for shadow areas. Color scaling was also performed on the images after the retinex algorithm. However, after the color scaling, some objects in images, especially soil under the canopy, had incorrect color. This false color was corrected by replacing the hue component (H) in the enhanced image with the original hue component in the HSV color space of the original image, and these composite images were used for the classification process. The composite images were denoted $HS'V'$, where S' and V' represent the enhanced saturation and value components after the retinex algorithm and color scaling. In order to analyze color information in different color spaces, the $HS'V'$ images were transformed to the RGB and the luminance, blue difference, and red difference

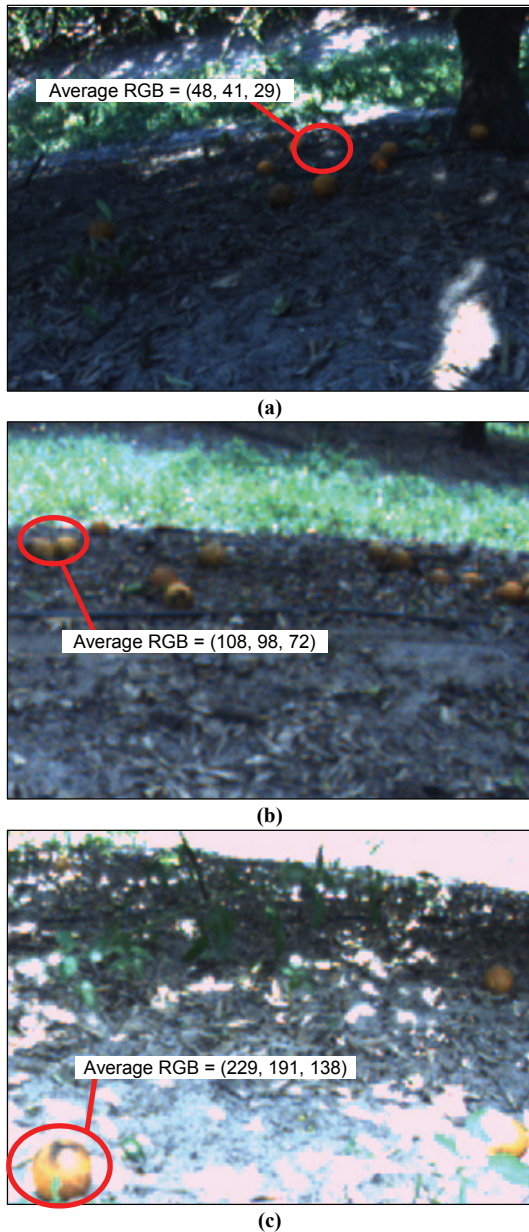


Figure 4. Color variation in citrus fruit based on illumination level. RGB values in boxes are averages of all citrus pixels inside circles: (a) dark image (average gray value = 38), (b) medium image (average gray value = 137), and (c) bright image (average gray value = 182).

chroma (YCbCr) color spaces, which were denoted as R'G'B' and Y'Cb'Cr', respectively. These different notations were used for the enhanced images to distinguish them from the original RGB and YCbCr values.

COLOR COMPONENT SELECTION FOR CLASSIFICATION

The training set (20 images for each illumination level) was used to collect the color information of different objects in the images. Two classes (non-fruit objects and citrus fruit) in the training set images were manually cropped using a Matlab program that was developed for this research. Pixel values of the fruit and the background in the R'G'B', HS'V', and Y'Cb'Cr' color spaces were collected for the three illumination levels. The criterion used to

choose optimal color components for classification was the sum of the Mahalanobis distances. Input arguments of the Mahalanobis distance function were the color values of object pixels and the class (fruit or non-fruit) collected from the training images. After calculating the Mahalanobis distances, the four highest components were chosen for use as the optimal features for classification because larger distance means better classification capability as it represents more variation in color values between the classes.

CITRUS FRUIT PIXEL CLASSIFICATION

To classify pixels in images into two classes (fruit and non-fruit), probabilistic classification methods were used. Three classifiers in the algorithm were compared: naïve Bayesian, k -nearest neighbor (kNN), and logistic regression. For the naïve Bayesian classifier, a posterior probability of class y_j for feature vector x and a decision criterion were defined by equations 3 and 4, respectively:

$$P(y_j|x) = \frac{P(x|y_j)P(y_j)}{\sum_{j=1}^2 P(x|y_j)P(y_j)} \quad (3)$$

$$Y \leftarrow \arg \max_j \frac{P(x|y_j)P(y_j)}{\sum_{j=1}^2 P(x|y_j)P(y_j)} \quad (4)$$

where y_j is the class variable (fruit or non-fruit), P is the probability function, x is the feature vector of the optimal color components from the feature selection [x_1, x_2, x_3, x_4], and Y is the output class.

The kNN classifier calculates the distance between the current feature vector to be classified and samples in the training set and chooses the nearest k samples for class selection. Based on preliminary tests, the Mahalanobis distance was used for distance calculation, and k was set to 5.

Lastly, the logistic regression classifier was defined by the probability density function given in equations 5 and 6:

$$P = \frac{1}{1 + e^{(w^T x + w_0)}}, \quad (P \in [0,1]) \quad (5)$$

$$Y = \begin{cases} 1 & \text{with probability } P \\ 0 & \text{with probability } 1 - P \end{cases} \quad (6)$$

where $w = [w_1, w_2, w_3]$, and w_0 are coefficients of the exponential function in the denominator of equation 5. In the classification algorithm, the classifiers processed each pixel in an image and assigned 0 to non-fruit pixels and 1 to citrus pixels. Input arguments of the probability function of the three classifiers were expressed as a vector ($x = [x_1, x_2, x_3, x_4]$) with the four optimal color components chosen from the feature selection. After classification, several operations, including thresholding, erosion, and dilation, were applied to remove noise. Threshold values to remove small pixels of noise were calculated from the training set by finding minimum areas of citrus fruit at different locations in the image because citrus fruits closer to the camera appeared larger than those farther away. Erosion and dilation were applied to remove the noise near fruit boundaries.

WATERSHED ALGORITHM AND h -MINIMA TRANSFORM

The images used in this study were acquired at a low height (50 cm) with a vertical field of view (actual size of area that the camera covers in the vertical direction) of more than 7 m. Consequently, on many occasions, fruit that were located far from the camera (i.e., in the upper half of images) appeared to overlap even though they were not actually overlapping in the field. The total count of citrus fruit was underestimated because the algorithm recognized overlapped fruits as one fruit. To segment overlapped fruit, the watershed algorithm was applied to the upper half of the images. The watershed algorithm is an edge-based segmentation technique that uses topographic gradients to find the boundaries of objects based on the regional minima and maxima of the topography (Roerdink and Meijster, 2000). However, the watershed algorithm often produces oversegmentation, generating excessive regional minima from an object. Therefore, the h -minima transform (Shin et al., 2012) was used to avoid oversegmentation with the watershed algorithm. The h -minima transform removes trivial regional minima in the image by specifying threshold h . In this study, the h value was chosen to be 4 from the training set to minimize oversegmentation. In figure 5, each circle represents one segment. Figure 5a shows one citrus fruit that has been overly segmented into two fruits. However, after the watershed algorithm with h -minima transform, the oversegmentation was suppressed, and only one citrus fruit is detected in figure 5b.

FRUIT COUNTING AND SIZE AND MASS ESTIMATION

To count the number of dropped fruits in an image, ellipse fitting was performed for each segmented object. The

number of fitted ellipses was considered the citrus fruit count. The ellipse fitting provided the centroid position and diameter, which was calculated from the average length of the major and minor axes, and these were used to determine the actual diameter of the fruit using a calibration model.

To model the relationship between actual fruit size and its size in an image, calibration images containing a total of 15 Styrofoam balls of three different diameters (6.4, 7.6, and 10.2 cm) were used. The calibration images were acquired indoors with the same camera angle and height used the field experiment (60° and 50 cm). The Styrofoam balls were placed at different locations to measure their diameter according to the distance from the camera. The diameters of the balls in the images according to their centroid position (row number in image) were measured, and the unit was number of pixels. A bilinear lookup table was created for the actual diameter, the centroid position, and the diameter in the images.

The estimated diameter of the citrus fruit was converted to mass based on another calibration model. A total of 43 citrus fruits ranging from small to large in size were collected from the field. The mass and diameter of each fruit were measured with a scale (Adventurer, Ohaus Corp., Pine Brook, N.J.) and caliper (Digimatic caliper, Mitutoyo Corp., Kanagawa, Japan), respectively. For each fruit, the major (long) and minor (short) diameters were measured, and an average of the two was calculated and used as the fruit size. A relationship between the mass and the average diameter was estimated by second-order polynomial curve fitting.

The performance of the citrus counting algorithm was analyzed in terms of two criteria: correct identification and false positives. Correct identification represents citrus objects properly detected by the algorithm, and false positives are non-citrus objects incorrectly identified as citrus fruit. Manual counting was conducted by two volunteers to determine the total number of fruit, the number of correct identifications, and the number of false positives in the validation images. For analysis of the mass estimation algorithm, a coefficient of determination was calculated between the mass estimated by the algorithm and the actual mass estimated from the manual counting.

RESULT AND DISCUSSION

COLOR VARIANCE WITH DIFFERENT ILLUMINATION

Histogram analysis confirmed the color variation in the training images (fig. 6). RGB histograms of citrus fruit pixels in the training set according to the image's illumination level show that the color values were significantly different under dark, medium, and bright illumination even though the objects were in the same class.

ILLUMINATION ENHANCEMENT USING RETINEX ALGORITHM

The retinex algorithm was applied to the images to reduce the variation in color values due to illumination level. An example of the resulting images for dark illumination is shown in figure 7. Although some grass was distinguishable, soil and tree bark were too dark to be recognized. The color

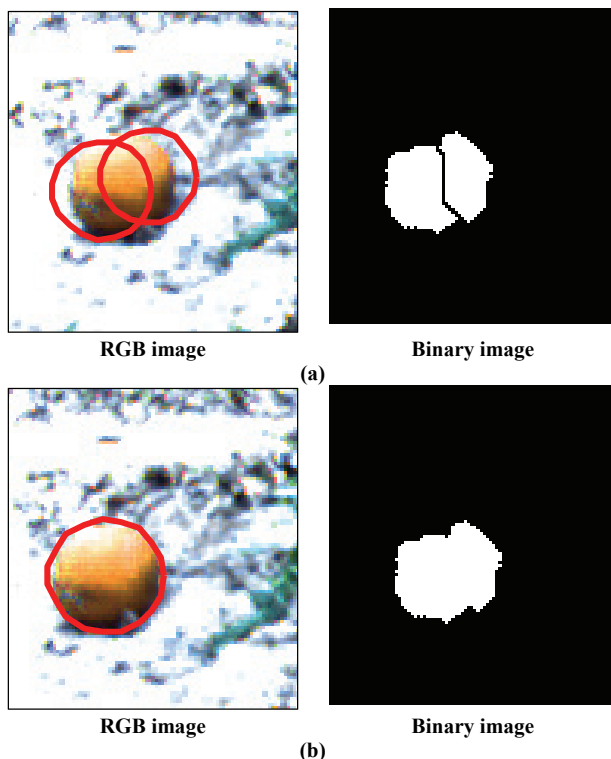


Figure 5. Watershed algorithm with h -minima transform: (a) over-segmentation of citrus fruit and (b) suppressed segmentation.

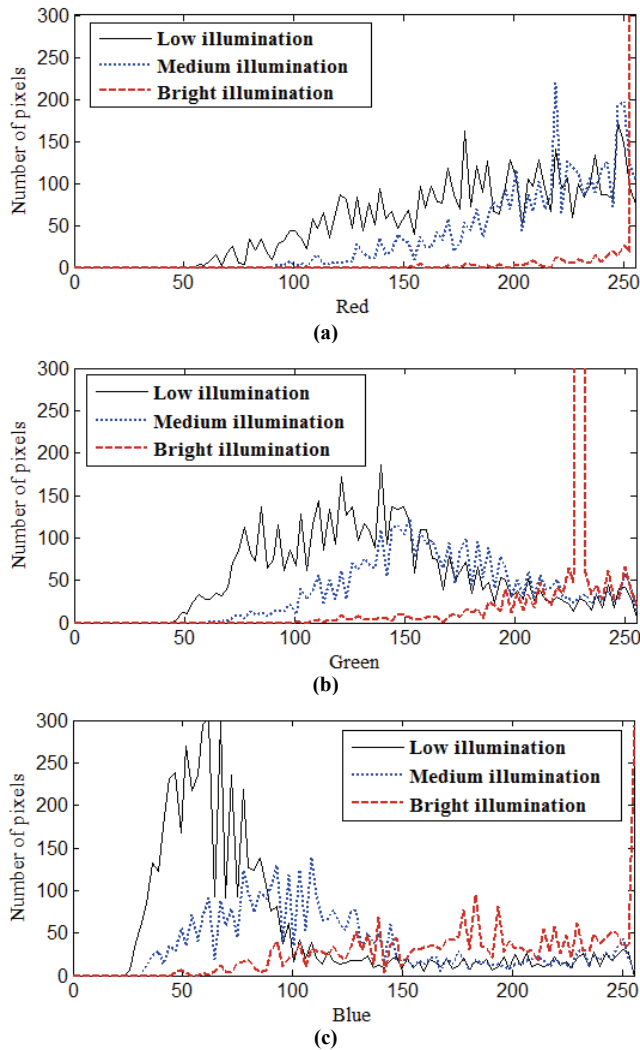


Figure 6. Color variation of citrus fruit in the (a) red, (b) green, and (c) blue components according to different illumination conditions.

of the citrus fruit was also faint orange with shades of brown and black (fig. 7a). After applying the retinex algorithm with a standard deviation of 250, the illumination was greatly enhanced (fig. 7b). However, the image had white shade from the retinex algorithm, and consequently the colors of objects in the image became lighter. To solve this problem, intensity values in the image were adjusted by color scaling, resulting in figure 7c. The retinex algorithm with a standard deviation of 50 was then applied to the image (fig. 7d). Illumination under the canopy area was enhanced, but the color values of objects in the image were changed incorrectly by the color scaling. The composite image (HS'V') is shown in figure 7e. In this image, the original color was restored by combining the original H component with the enhanced S' and V' components, and the color values of the citrus fruit were enhanced enough to be distinguishable.

An example of the retinex algorithm applied to a medium illumination image is shown in figure 8. For these images, the retinex algorithm was applied with a standard deviation value of 50. The original image is shown in figure 8a. After applying the retinex algorithm, the illumination was enhanced, but color was biased during the color

scaling (fig. 8b). In the composite image (HS'V') in figure 8c, the citrus fruit became more distinguishable compared to the original image.

For a bright illumination image (fig. 9), the retinex algorithm was applied section by section (20×640 pixels). Based on the illumination level of each section (shadow or non-shadow), different c values were applied. For shadow areas, the retinex algorithm was applied twice with different c values, first 250 and then 50 (the same as for the dark image in fig. 7) to enhance dark areas. For non-shadow areas, the standard deviation was 50. In the composite image in figure 9c, the colors of citrus fruits in shadow areas and in bright areas became similar.

The illumination levels (average gray values) of the original images before enhancement varied in a wide range between images. Figure 10a shows the range of the average gray values of the 120 original images in the validation set. The average values ranged from 31 to 218 and were distributed almost evenly across the entire range. However, the difference in illumination levels between images decreased significantly after enhancement. Figure 10b shows that the average gray values ranged from 131 to 186 after enhancement, so that all the images had medium-bright illumination levels.

COLOR COMPONENT SELECTION FOR CLASSIFICATION

The four components with the greatest Mahalanobis distances were selected for use in the classification. For the dark and medium illumination images, the H, S', Cb', and Cr' components were selected. For the bright illumination images, the R', H, Cb', and Cr' components were used for classification (fig. 11).

CITRUS PIXEL CLASSIFICATION

Classification results from the logistic regression model for dark, medium, and bright images are shown in figures 12, 13, and 14, respectively. Images enhanced by the retinex algorithm are shown in figures 12a, 13a, and 14a; the original images for the three illumination levels are the same as figures 7a, 8a, and 9a. After the classification, binary images were generated, as shown in figures 12b, 13b, and 14b. In the binary images, citrus pixels are represented as white pixels, and non-fruit pixels are represented as black pixels. To remove noise after classification, thresholding in area, erosion, and dilation were applied. The threshold value was determined based on the minimum areas of citrus fruit in the training set, which were 18, 121, and 293 pixels for rows 1 to 160, 161 to 320, and 321 to 480, respectively. The watershed algorithm with h -minima transform was then used to segment overlapped citrus fruit (figs. 12d, 13d, and 14d).

CITRUS FRUIT MASS ESTIMATION

In the calibration images, the size of the Styrofoam balls in the images increased linearly as the actual size of the balls increased at the same distance from the camera. Additionally, for the same size of ball, the size of the ball in the images had a linearly decreasing relationship as the distance from the camera increased. Table 1 was used as a



Figure 7. Example of the retinex algorithm applied to a dark illumination image: (a) original image, (b) retinex with $c = 250$ resulting in a white shade problem, (c) image after color scaling, (d) second retinex with $c = 50$, and (e) R'G'B' image converted from composite image (HS'V').

lookup table for estimating the actual fruit size given the centroid position and the diameter of the fruit in the image. Using table 1, unspecified values of centroid position (row number) and fruit size (number of pixels) were estimated by linear interpolation. Table 2 shows the accuracy test results for size estimation using the lookup table (table 1). Root mean square errors (RMSE) between estimated sizes and actual sizes were measured using 15 Styrofoam balls of three different sizes (6.4, 7.6, and 10.2 cm). The average RMSE of 15 measurements was 0.12 cm, with a maximum RMSE of 0.25 cm and minimum RMSE of 0.01 cm.

The estimated size of the citrus fruit was converted into mass using a model from another calibration data set be-

tween actual diameter and mass for a set of 43 citrus fruit. The relationship between mass and average diameter was estimated by second-order polynomial curve fitting (eq. 7, fig. 15):

$$\text{Mass} = 18.88d^2 - 187.3d + 576.3 \quad (7)$$

where d is the average fruit diameter.

ACCURACY OF COUNTING AND MASS ESTIMATION

Classification using the naïve Bayesian, kNN, and logistic regression classifiers was conducted, and their classification accuracies were compared. Two volunteers were recruited to manually count fruits in the images identified by each classifier. The actual number of fruit in the images



(a)



(b)



(c)

Figure 8. Example of the retinex algorithm applied to a medium illumination image: (a) original image, (b) retinex with $c = 50$, and (c) R'G'B' image converted from composite image (HSV').

was 1492 by the first manual counting and 1502 by the second manual counting. In table 3, the third to fifth columns represent the results from the manual counting of fruits in the images by the first volunteer, and the sixth to eighth columns represent the results from the manual counting by the second volunteer. For each manual counting, the columns represent the number of fruit correctly identified by the algorithm, the coefficient of determination (R^2) between the count of fruit detected by the algorithm and the actual number of fruit, and the false positives. The percentages are also listed with respect to the actual number of fruit. For example, for the Bayesian classifier, the percentage of correctly identified fruit and the false positives for the first manual counting were calculated by $100 \times 1240/1492$ and $100 \times 285/1492$, respectively. Even though



(a)



(b)



(c)

Figure 9. Example of the retinex algorithm applied to a bright illumination image: (a) original image, (b) retinex applied by section, and (c) final result after color restoration.

the values for the two manual countings were slightly different, the logistic regression classifier performed best compared to both manual countings. The percentage of correctly identified fruit was 88.1% for both manual countings. Most of the missed fruits were from small objects in the images that did not contain enough information, such as color and shape, to be detected.

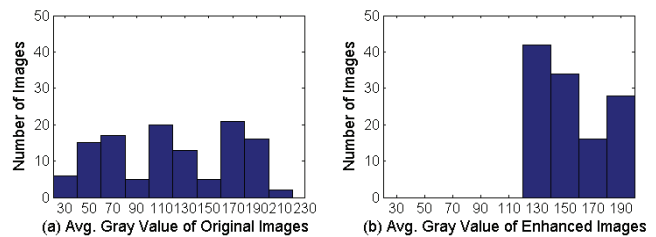


Figure 10. Histograms of average gray values (overall illumination levels) of images: (a) original images in the validation set and (b) images after enhancement.

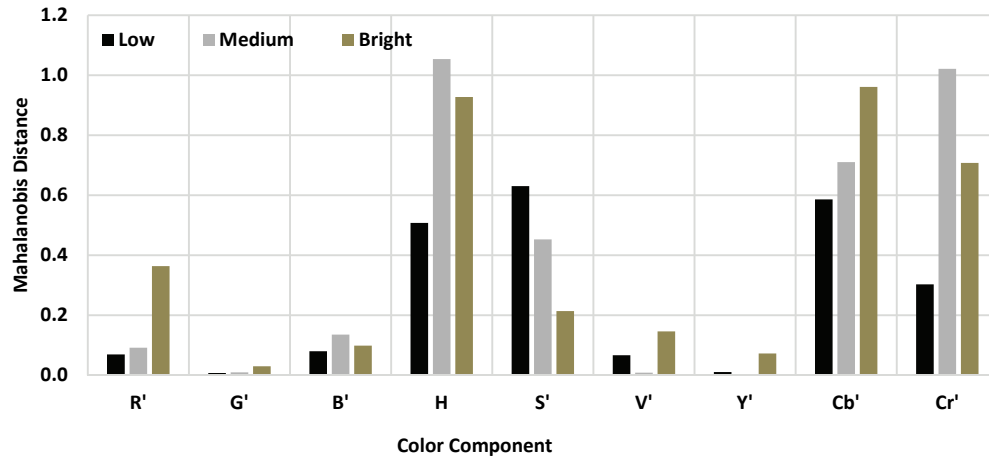


Figure 11. Sum of Mahalanobis distance of each color component for feature selection.

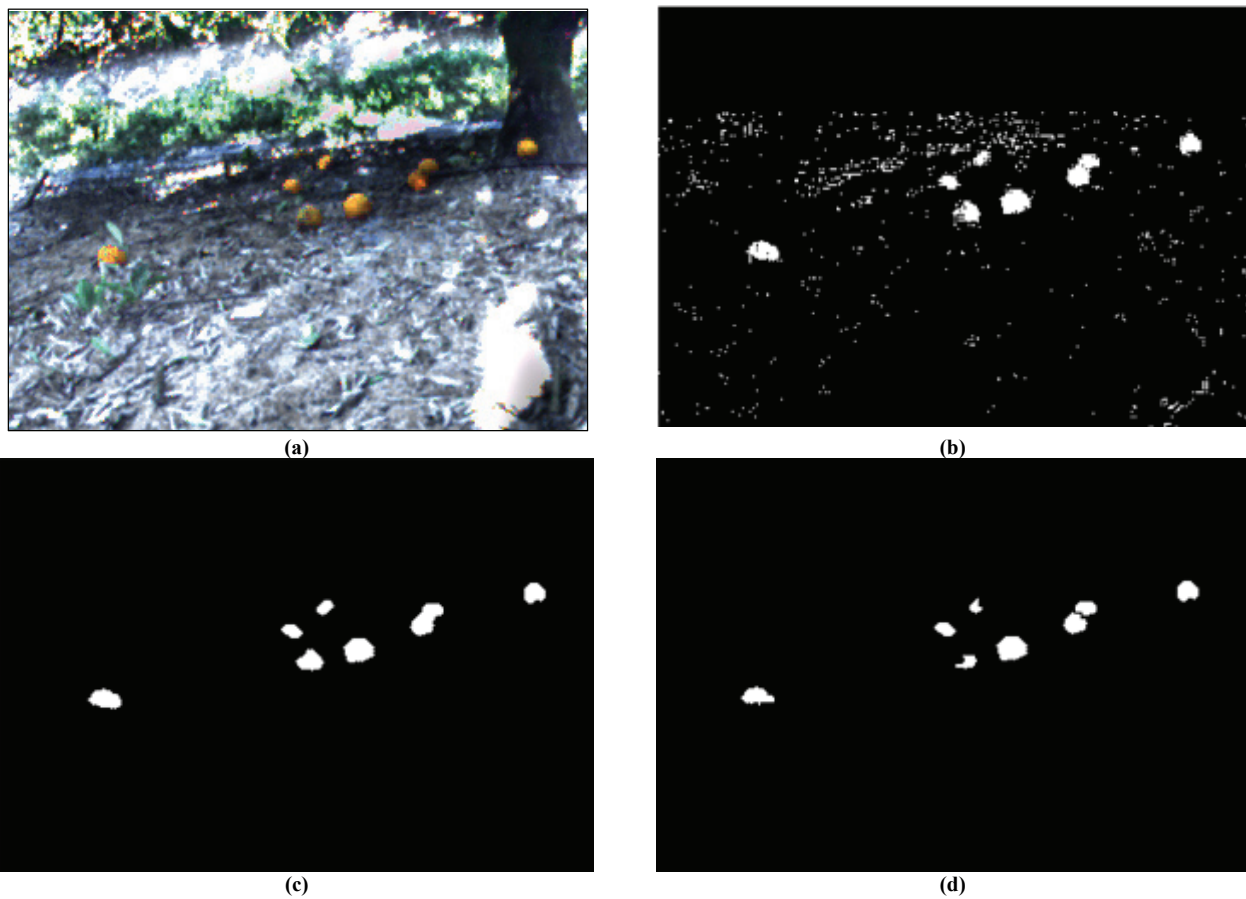


Figure 12. Citrus fruit detection for a dark illumination image: (a) image enhanced with retinex algorithm (same image as fig. 7e), (b) result of classification (white pixels represent citrus fruit), (c) noise removal, and (d) final result after watershed algorithm with h -minima transform.

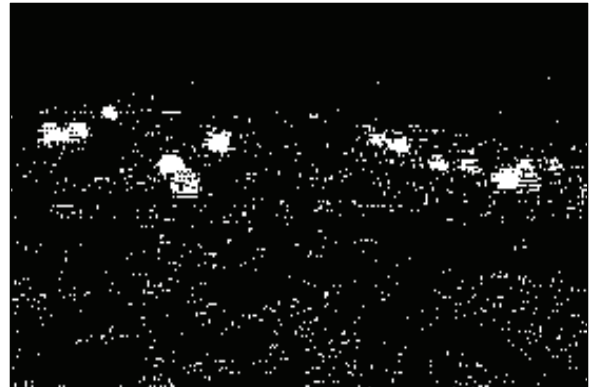
The false positive rate was high for the kNN classifier. This was because grass and leaves in bright areas tended to have yellowish colors that were similar to citrus fruit. The kNN classifier was strongly affected by data density in the boundary areas and correspondingly had poor discrimination ability. Another source of false positives for all three classifiers was the watershed segmentation. Oversegmentation still occurred even though the h -minima transform was performed. Many of the detected citrus fruits were of ran-

dom shape because the fruit was overlapped by grass or leaves, partly hidden by soil, or crushed by other vehicles or animals in the field. The random shape of these citrus fruits caused excessive segmentation and multiple counting of single fruits.

The estimated mass after fruit detection is shown in table 4. A regression analysis was performed between the actual mass estimated from both manual countings and the



(a)



(b)



(c)



(d)

Figure 13. Citrus fruit detection for a medium illumination image: (a) image enhanced with retinex algorithm (same image as fig. 8c), (b) result of classification (white pixels represent citrus fruit), (c) noise removal, and (d) final result after watershed algorithm with h -minima transform.



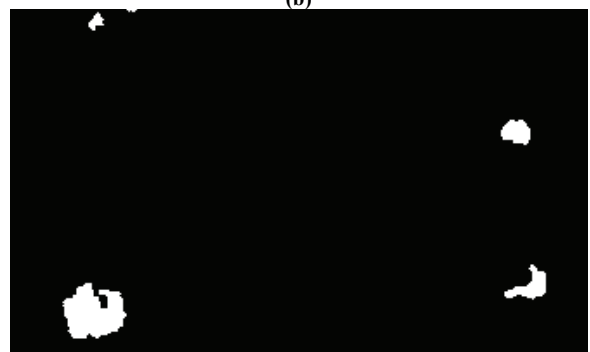
(a)



(b)



(c)



(d)

Figure 14. Citrus fruit detection for a bright illumination image: (a) image enhanced with retinex algorithm (same image as fig. 9c), (b) result of classification (white pixels represent citrus fruit), (c) noise removal, and (d) final result after watershed algorithm with h -minima transform.

Table 1. Part of a lookup table for bilinear relationship between actual fruit size in image and centroid position.

Centroid Position (row number)	Actual Size of Citrus Fruit		
	6.4 cm	7.6 cm	10.2 cm
40	12.9	16.2	17.5
80	18.1	20.0	25.6
120	22.9	24.3	32.7
160	25.1	29.0	39.7
200	29.2	34.6	46.8
240	33.2	40.1	54.0
280	37.3	45.7	61.1
320	41.3	51.3	68.3
360	45.4	56.9	75.4
400	49.4	62.5	82.5
440	53.5	68.1	89.7
480	57.5	73.7	96.8

Table 2. Accuracy analysis for size estimating lookup table (LUT) using centroid position and diameter in an image.

Actual Size of Styrofoam Ball (cm)		Centroid Position in Image (row number)	Estimated Size by LUT (cm)	RMSE between Actual and Estimated Size	Overall Average RMSE
6.4	30.9	223	6.22	0.13	
	19.8	95	6.28	0.07	
	25.1	167	6.15	0.20	
	17.2	73	6.34	0.01	
	23.4	124	6.53	0.18	
7.6	36.9	218	7.60	0.02	
	29.0	161	7.57	0.05	
	21.2	94	7.41	0.21	
	24.7	124	7.55	0.07	
	19.3	73	7.59	0.03	
10.2	49.9	212	10.34	0.18	
	39.7	158	10.27	0.11	
	28.2	91	10.41	0.25	
	33.2	121	10.25	0.09	
	24.1	71	10.33	0.17	

mass estimated from the images. The coefficients of determination (R^2) for the three classification methods were 0.62, 0.59, and 0.69 for the first manual counting and 0.62, 0.58, and 0.69 for the second manual counting. The R^2 values of the estimated mass were reduced due to the false positives from the classification. In addition, the position information estimated during the mass estimation process was not accurate because only a single camera was used. Position was one of the most important factors for estimating the actual size of the fruit. Because the mass of the fruit was estimated based on the estimated size, the estimated mass led to inaccurate results. The cameras were also installed on a moving vehicle, and it was difficult to maintain a constant distance between the cameras and the citrus fruit due to the varying size of the citrus trees.

The results of this study demonstrate the prototype sys-

Table 3. Performance analysis based on correctly identified citrus fruit and false positives. The actual number of fruit in the images was 1492 by the first manual counting and 1502 by the second manual counting, and the average was 1497. Values are numbers of fruit (with percentages in parentheses).

Classifier	Count by Algorithm	First Manual Counting 1			Second Manual Counting 2			Average		
		Correctly Identified	R^2	False Positives	Correctly Identified	R^2	False Positives	Correctly Identified	R^2	False Positives
Bayesian	1525	1240 (83.1)	0.76	285 (19.1)	1241 (82.6)	0.75	284 (18.9)	1240.5 (82.9)	0.75	284.5 (19.0)
kNN	1866	1251 (83.8)	0.61	615 (41.2)	1255 (83.6)	0.60	611 (40.7)	1253 (83.7)	0.61	613 (40.9)
Logistic regression	1525	1314 (88.1)	0.87	211 (14.1)	1324 (88.1)	0.87	201 (13.4)	1319 (88.1)	0.87	206 (13.8)

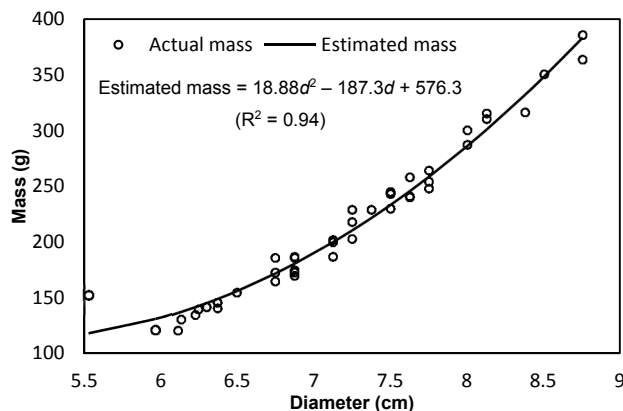


Figure 15. Regression of the actual size and mass of citrus fruit.

tem's ability to quantify early citrus fruit drop at different locations. The mass estimation had reduced performance due to the false positives and inaccurate estimation of the distance between the camera and the citrus fruits. However, the estimation of the dropped fruit count showed similar or better results compared to other studies in outdoor environments. The results from the algorithm using the logistic regression classifier showed that the R^2 value between the count of dropped fruit and the actual number of fruit was 0.87. Other reported R^2 values were 0.76 by Annamalai and Lee (2003), 0.79 by Annamalai et al. (2004), and 0.83 to 0.88 by Stajanko et al. (2004). For correctly identified citrus fruit, this study showed a much higher rate (88.1%) than Patel et al. (2012), who reported 69% (i.e., a 31% error rate).

Figure 16 shows the quantified early citrus fruit drop at different locations with excessive and fewer fruit drop regions as a geo-referenced spatial variability map by combining DGPS coordinates with the amount of fruit drop per unit area. Such spatial variability maps of fruit drop will help growers find problematic areas in their groves more easily.

Further performance improvement can have two approaches: (1) improvement of the image acquisition system, and (2) improvement of the image processing algorithm. The low-resolution cameras used in the current system can be replaced with higher-resolution cameras or a video camera to avoid low-quality images and unnecessary triggering time. In addition, the single-scale retinex algorithm with color scaling can be improved by using a multi-scale retinex algorithm with color restoration (MSRCR). The MSRCR is often considered an efficient method for enhancing images; however, choosing parameters for the MSRCR is challenging because there are no standard rules.

Table 4. Regression analysis for mass estimation by the three classifiers. R² values were calculated between mass by estimated the classifiers and actual mass estimated from each manual counting.

Classifier	Estimated Mass (kg)	R ² Value	
		First Manual Counting	Second Manual Counting
Bayesian	811.0	0.62	0.62
kNN	1035.1	0.59	0.58
Logistic regression	805.4	0.69	0.69

CONCLUSION

A machine vision system was developed for counting and estimating the mass of dropped citrus fruit on the ground during harvest. The image processing algorithm consisted of: (1) illumination enhancement using retinex theory, (2) classification, (3) watershed algorithm with the *h*-minima transform and (4) ellipse fitting for citrus count and mass estimation. The main achievements of this study were:

1. Illumination enhancement algorithm: The retinex algorithm reduced the effect of varying illumination conditions, which is the main problem in outdoor imaging. In the original images, the illumination level varied widely from very dark (average intensity of 30) to very bright (average intensity of 210). After enhancement, the illumination and colors of citrus fruit became similar regardless of the original illumination level. This algorithm was also shown to enhance classification ability during feature selection by increasing the variance in colors between citrus fruit and background objects.

2. Mass estimation using ellipse fitting: Citrus fruit segmented using the watershed algorithm with *h*-minima were fitted to ellipses, and the diameter of each ellipse was converted to mass based on two calibration models. The accuracy of the mass estimation can be improved by improving the imaging devices.
3. Quantification of citrus fruit drop and creation of fruit drop map: The amount of fruit drop with geo-referenced location information can be correlated with HLB intensity data, psyllid counts, fertilization programs, and other block-specific management practices to allow more efficient management of HLB-infected blocks.

For an extension of this research, a machine vision system using multiple video cameras with HD resolution (1080p) is currently being developed. For future work, the machine vision system developed in this research can be extended by implementation as a real-time system that can be used easily in a commercial citrus grove.

ACKNOWLEDGEMENTS

This project was supported by the Citrus Initiative program of the University of Florida Institute of Food and Agricultural Sciences. The authors would like to thank Mr. Michael Zingaro, Dr. Alireza Pourreza, Dr. Mazin Saber, Dr. Mahmoud Khedher Agha, Dr. Ce Yang, Dr. Han Li, Ms. Chuanyuan Zhao, Mr. Chuanqi Xie, Ms. Mubarkat Shuaibu, and Ms. Brianna Posadas at the University of Florida for their assistance in this research.

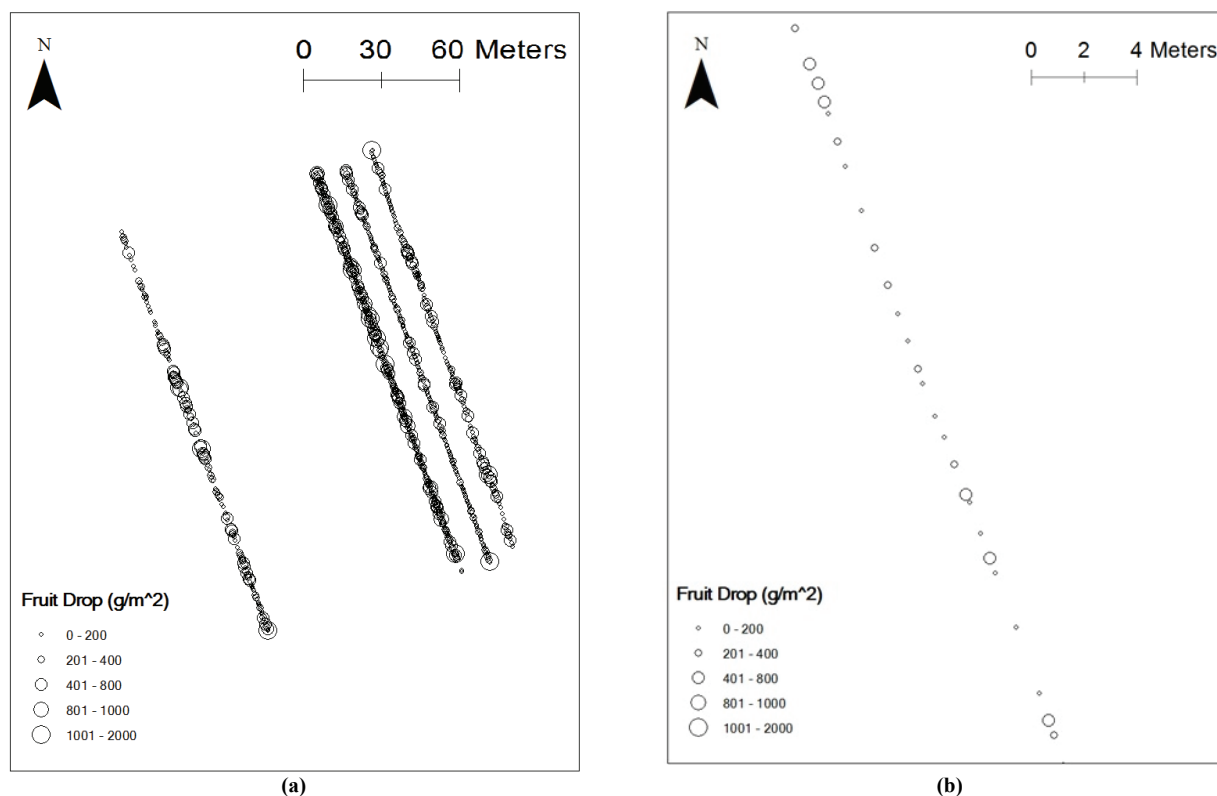


Figure 16. Geo-referenced fruit drop map: (a) distant view showing four different tree rows and (b) zoomed view showing one tree row.

REFERENCES

- Aleixos, N., Blasco, J., Navarron, F., & Molto, E. (2002). Multispectral inspection of citrus in real-time using machine vision and digital signal processors. *Computers Electronics Agric.*, 33(2), 121-137. [http://dx.doi.org/10.1016/S0168-1699\(02\)00002-9](http://dx.doi.org/10.1016/S0168-1699(02)00002-9).
- Annamalai, P., & Lee, W. S. (2003). Citrus yield mapping system using machine vision. ASAE Paper No. 031002. St. Joseph, Mich.: ASAE. <http://dx.doi.org/10.13031/2013.13701>.
- Annamalai, P., Lee, W. S., & Burks, T. F. (2004). Color vision system for estimating citrus yield in real-time. ASAE Paper No. 043054. St. Joseph, Mich.: ASAE. <http://dx.doi.org/10.13031/2013.16714>.
- Bassanezi, R. B., Montesino, L. H., Gasparoto, M. C., Filho, A. B., & Amorim, L. (2011). Yield loss caused by Huanglongbing in different sweet orange cultivars in São Paulo, Brazil. *European J. Plant Pathol.*, 130(4), 577-586. <http://dx.doi.org/10.1007/s10658-011-9779-1>.
- Begeman, J., & Wright, G. (2009). Diagnosing home citrus problems. Tucson, Ariz.: University of Arizona Cooperative Extension. Retrieved from <http://ag.arizona.edu/pubs/crops/az1492.pdf>.
- Chinchuluun, R., Lee, W. S., & Ehsani, R. (2009). Machine vision system for determining citrus count and size on a canopy shake and catch harvester. *Appl. Eng. Agric.*, 25(4), 451-458. <http://dx.doi.org/10.13031/2013.27459>.
- HunterLab. (2012). Measuring color using Hunter *L, a, b* versus CIE *L*, a*, b**. Reston, Va.: Hunter Associates Laboratory. Retrieved from www.hunterlab.com/an-1005b.pdf.
- Li, H., Lee, W. S., Wang, K., Ehsani, R., & Yang, C. (2014). Extended spectral angle mapping (ESAM) for citrus greening disease detection using airborne hyperspectral imaging. *Precision Agric.*, 15(2), 162-183. <http://dx.doi.org/10.1007/s11119-013-9325-6>.
- Ling, P., Ehsani, R., Ting, K., Chi, Y., Ramalingam, N., Klingman, M., & Draper, C. (2004). Sensing and end-effector for a robotic tomato harvester. ASAE Paper No. 043088. St. Joseph, Mich.: ASAE. <http://dx.doi.org/10.13031/2013.16727>.
- Patel, H. N., Jain, R. K., & Joshi, M. V. (2012). Automatic segmentation and yield measurement of fruit using shape analysis. *Intl. J. Computer Applic.*, 45(7), 9-24.
- Pourreza, A., Lee, W. S., Raveh, E., Hong, Y., & Kim, H. J. (2013). Identification of citrus greening disease using a visible band image analysis. ASABE Paper No. 131591910. St. Joseph, Mich.: ASABE. <http://dx.doi.org/10.13031/aim.20131591910>.
- Rahman, Z. (1995). Properties of a center/surrounded retinex: Part 1. Signal processing design. NASA Contractor Report 198194. Hampton, Va.: NASA Langley Research Center.
- Roerdink, J., & Meijster, A. (2000). The watershed transform: Definitions, algorithms, and parallelization strategies. *Fundamenta Informaticae*, 41(1-2), 187-228.
- Shin, J. S., Lee, W. S., & Ehsani, R. (2012). Postharvest citrus mass and size estimation using a logistic classification model and a watershed algorithm. *Biosyst. Eng.*, 113(1), 42-53. <http://dx.doi.org/10.1016/j.biosystemseng.2012.06.005>.
- Stajanko, D., Lakota, M., & Hočevar, M. (2004). Estimation of number and diameter of apple fruits in an orchard during the growing season by thermal imaging. *Computers Electronics Agric.*, 42(1), 31-42. [http://dx.doi.org/10.1016/S0168-1699\(03\)00086-3](http://dx.doi.org/10.1016/S0168-1699(03)00086-3).
- USDA. (2014). Citrus: World market and trade. Washington, D.C.: USDA Foreign Agricultural Service. Retrieved from www.fas.usda.gov/psdonline/circulars/citrus.pdf.
- Yang, C., Lee, W. S., & Williamson, J. G. (2012). Classification of blueberry fruit and leaves based on spectral signatures. *Biosyst. Eng.*, 113(4), 351-362. <http://dx.doi.org/10.1016/j.biosystemseng.2012.09.009>.
- Zekri, M., & Rouse, R. E. (2013). Citrus problems in the home landscape. Publication HS876. Gainesville, Fla.: University of Florida Institute of Food and Agricultural Sciences. Retrieved from <http://edis.ifas.ufl.edu/hs141>.